Contribution of Tropical Cyclones to the Global Precipitation from Eight Seasons of TRMM Data: Regional, Seasonal, and Interannual Variations

HAIYAN JIANG

Department of Earth and Environment, Florida International University, Miami, Florida

EDWARD J. ZIPSER

Department of Atmospheric Sciences, University of Utah, Salt Lake City, Utah

(Manuscript received 19 June 2009, in final form 2 October 2009)

ABSTRACT

Based on the University of Utah Tropical Rainfall Measuring Mission (TRMM) precipitation feature (PF) database, tropical cyclone PFs (TCPFs) are identified for over 600 storms that reached tropical storm intensity level or above around the globe during eight TC seasons from the period of 1998–2006. Each TC season includes 6 months yr^{-1}. Six basins are considered: Atlantic (ATL), east-central Pacific (EPA), northwest Pacific (NWP), north Indian Ocean (NIO), south Indian Ocean (SIO), and South Pacific (SPA). TRMM 2A25- (precipitation radar) and 3B42- (multisatellite) derived rainfall amounts are used to assess the impact of tropical cyclone (TC) rainfall in altering the regional, seasonal, and interannual distribution of the global total rainfall during the TC seasons in the six basins. The global, seasonal, and interannual variations of the monthly rainfall inside TCPFs are presented. The fractional rainfall contributions by TCPFs are compared in different basins. The TRMM 2A25 and 3B42 retrievals are compared in terms of the rainfall contribution by TCs. After constraining TC rainfall for being within 500 km from the TC center, 2A25 and 3B42 show similar results: 1) TCs contribute, respectively, 8%–9%, 7%, 11%, 5%, 7%–8%, and 3%–4% of the seasonal rainfall to the entire domain of the ATL, EPA, NWP, NIO, SIO, and SPA basins; 2) both algorithms show that, regionally, the maximum percentage of TC rainfall contribution is located in EPA basin near the Mexico Baja California coast (about 55%), SIO close to the Australia coast (about 55%), and NWP near Taiwan (about 35%–40%); 3) the maximum monthly percentage of TC rainfall contribution is in September for the ATL basin, August and September for EPA, August for NWP, May for NIO, March for SIO, and January and February for SPA; 4) the percentage of rainfall contributed by TCs is higher during El Niño years than La Niña years for EPA and NWP basins. The trend is the reverse for ATL and NIO, and nearly neutral for SIO and SPA. However, this study does not include enough years of data to expect the findings to be representative of long-term statistics of the interannual variations.

1. Introduction

Tropical cyclones (TCs) have a great impact on the total precipitation over global ocean basins. Since the latent heat release by cloud and precipitation is one of the main driving forces of the general atmospheric circulation (Mutai and Ward 2000; Gan et al. 2004), quantitative information about the contribution of TCs in distributing rainfall is critical to understanding the impact of these systems in altering the seasonal and global pattern of the general circulation.

The contribution of TCs to cumulative precipitation has been investigated in regions like the whole North Pacific (Rodgers et al. 2000) and North Atlantic (Rodgers et al. 2001) basins, the western North Pacific (Kubota and Wang 2009), China including Taiwan and the Hainan Islands (Ren et al. 2006), four minibasins near coastal southeastern Unites States (Shepherd et al. 2007), and China's Hainan Island only (Wu et al. 2007). Larson et al. (2005), using gridded daily rainfall analysis based on rain gauge observations, found that landfalling TCs contribute up to 15%–20% of rainfall along the U.S. Gulf and Mexican coasts on average during the period of 1950–98. Using rain gauge data over China during 1971–2004, Ren et al. (2006) determined that the ratio of annual TC precipitation to total annual rainfall is

Corresponding author address: Dr. Haiyan Jiang, 11200 SW 8th Street, PC-342B, Miami, FL 33199.
E-mail: haiyan.jiang@fiu.edu

DOI: 10.1175/2009JCLI3303.1

20%–30% in most of Taiwan and the China coastline south of 25°N, 30%–40% in most of Hainan and some locations of Taiwan and the coastline, and 40%–45% in southernmost Taiwan and westernmost Hainan. Kubota and Wang (2009) analyzed rainfall data at 22 rain gauge stations and found that along 125°E the TC rainfall accounts for 50%–60% of the total rainfall between 18° and 26°N during peak TC season from July to October. Wu et al. (2007) showed that TCs accounted for more than one-third of the total rainfall over the Hainan Island, China, for the period 1962–2005. Using monthly passive microwave rainfall estimates over two oceanic basins, Rodgers et al. (2000, 2001) determined that TCs contribute 7% (3%–4%) to the North Pacific (North Atlantic) cumulative rainfall. Maximum contributions of 30%–40% are found over coastal regions like the northeast of the Philippine Islands, lower Baja California coast, and northeast of Puerto Rico. Using Tropical Rainfall Measuring Mission (TRMM; Kummerow et al. 1998) measurements, Yokoyama and Takayabu (2008) calculated the rainfall contribution of TCs to total annual rainfall between 35°N and 35°S as 3.3%. The variation in the fraction of TC rain in different regions implies that the contribution of TC rain to total precipitation varies across the global oceans. Since existing studies are mostly regional, questions remain concerning the global amount that TCs contribute to the total rainfall, how these contributions are different for different global TC basins, and how TC rainfall patterns are distributed geographically, seasonally, and interannually.

In addition, above-mentioned studies use either rain gauge observations or satellite-based passive microwave estimates to examine the TC rainfall contribution. The reality is that different estimates could have different uncertainties. One of the main goals of the TRMM satellite is to quantify the distribution and variability of precipitation over the tropics and subtropics (Simpson et al. 1988). With the first-ever satellite-based precipitation radar (PR), TRMM provides invaluable measurements for global precipitation estimates (Adler et al. 2000; Schumacher and Houze 2003). Several algorithms use the TRMM satellite to make rainfall estimates. The PR-based 2A25 algorithm (Iguchi et al. 2000) is perhaps the best available rainfall estimates for both over ocean and over land systems in terms of its accuracy because of its active remote sensing characteristics. Better agreement has been found between PR 2A25 estimates and Global Precipitation Climatology Centre (GPCC) gauge rainfall than TRMM Microwave Imager (TMI) 2A12 estimates (Nesbitt et al. 2004). However, because of the narrow swath of the PR (215/247 km before–after TRMM boost on August 2001), TCs usually are not fully viewed by the TRMM PR (Fig. 4). In contrast, the TRMM Multisatellite Precipitation Analysis (TMPA, also referred to as TRMM 3B42; Huffman et al. 2007) provides a quasi-global (50°S–50°N) coverage of rain estimates at 3 hourly and $0.25° \times 0.25°$ resolution by combining all available satellite microwave measurements including TRMM and IR observations, although its estimates are subject to errors introduced by the IR-based rainfall retrieval.

In this study, we address the following questions: 1) what are the differences between the global TC rain fractions using the TRMM PR 2A25 and multisatellite 3B42 estimates; 2) how much rainfall is contributed by TCs to tropical and subtropical regions; 3) where and when does the greatest percentage contribution of TC rainfall occur; and 4) what are the influences of El Niño–Southern Oscillation (ENSO) on the TC rainfall pattern?

In the following sections, monthly TC rainfall and the rainfall generated by all other systems is determined using TRMM 2A25 and 3B42 data during 1998–2006. Estimates of TC and non-TC rainfall are compared between 2A25 and 3B42. Then the 2A25 monthly rainfall is used to examine global, seasonal, and interannual variations of global TC rain contribution.

2. Data and methodology

a. TRMM TCPF database

The University of Utah (UU) TRMM database is based on the framework of precipitation features (PFs) that were defined by grouping contiguous pixels based on certain criteria as observed by TRMM (Nesbitt et al. 2000; Liu et al. 2008). For example, Nesbitt et al. (2000) selected contiguous areas with near-surface reflectivity equal to or greater than 20 dBZ, or 85-GHz polarization corrected temperature (PCT; Spencer et al. 1989) equal to or less than 250 K as PFs. It provides an easy tool to search and sort a cloud/precipitation event based on its TRMM observed properties such as the feature size, volumetric rain, maximum 20-dBZ height, etc. Many regional and global climatological studies (Cecil et al. 2005; Zipser et al. 2006; Liu et al. 2008) of precipitation and convection, including TC studies (Cecil et al. 2002; Cecil and Zipser 2002), have been done using this database. The current UU TRMM PF database contains three levels of processing of TRMM data (see Liu et al. 2008 for details).

To study TCs specially, a TRMM tropical cyclone related precipitation feature (TCPF) database is created as a subset of the UU TRMM PF database. Our approach utilizes a distance threshold to define a TCPF. That is, we require the distance between the center of the tropical cyclone, according to best-track information, and the center of the PF at the time of TRMM observation to be less than 500 km. Here the PF center is

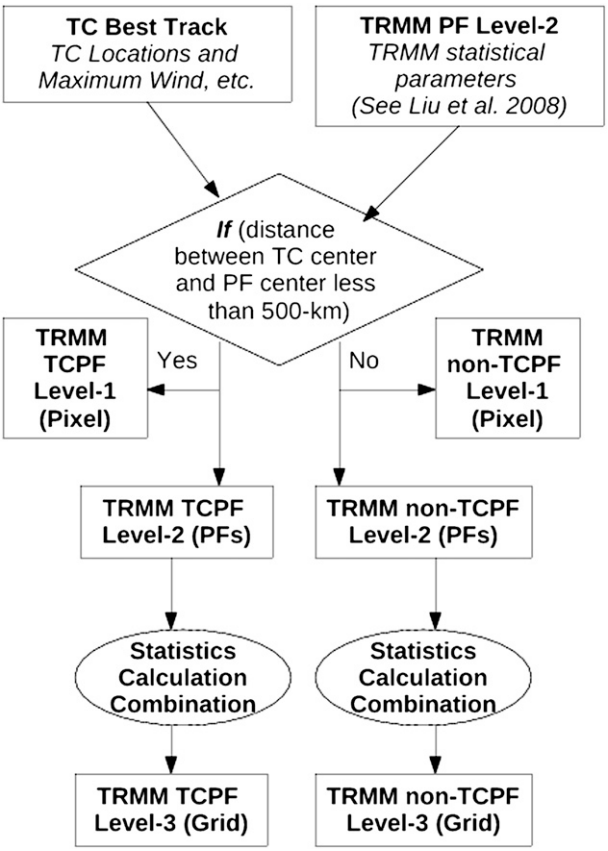

FIG. 1. TRMM TCPF database construction flowchart.

a raw geometric center, not being weighted by rain rates. TCPFs and non-TCPFs are separated. The construction of three levels of TCPF and non-TCPFs data is shown in Fig. 1. A similar procedure is used to create the 3B42 PF dataset. Level 1 data are produced in pixel-level parameters from the version 6 2A25 (Iguchi et al. 2000) and 3B42 granules, and TCPF and non-TCPF grouping. The output data are saved for each satellite orbit for TRMM PFs and for each 3-hourly analysis for 3B42 PFs. Using level 1 data, the statistics—such as mean, median, and volumetric rain—for each TCPF and non-TCPF are derived. Then, a monthly combination of orbital data is performed to obtain the level 2 TCPF and non-TCPF data. To process level 3 data, the monthly statistics of PF properties in level 2 data are derived on a $1° \times 1°$grid. The UU TRMM PF database also saves other parameters and contains several PF definitions (grouping methods; Liu et al. 2008). In this study, the PFs are defined as contiguous areas of surface raining pixels.

b. TC season and TRMM 2A25 global sampling

TCs occur mainly in TC seasons, which are different for different basins. Six basins are considered in this study, which include North Atlantic (ATL), east-central Pacific (EPA), northwest Pacific (NWP), north Indian Ocean (NIO), south Indian Ocean (SIO), and South Pacific (SPA). The analysis area for this study covers both land and ocean regions of the six basins. (The boundaries between basins are indicated in Figs. 3 and 4c). Please note that the central North Pacific region between 170°E and 160°W is omitted purposely to make the TC rain fractions more meaningful by excluding times and places where TCs rarely occur. Figure 2 shows the monthly TC numbers in each basin during 1998–2006 derived from National Hurricane Center (NHC) and Joint Typhoon Warning Center (JTWC) best-track data. From Fig. 2 we find that the TC number peaks in summer months for all basins except NIO, where TCs tend to occur in the monsoon transition months of early (May–June) and late in the wet season (October–November). Therefore, the TC seasons and analysis periods that we used in this study for each basin are 1) for the Northern Hemisphere, the 6-month period of June–November for ATL, EPA, and NWP and January, May–June, and October–December for NIO during the years of 1998–2000 and 2002–06 (TRMM satellite boost was in 2001 that caused some data problems in August 2001); and 2) for the Southern Hemisphere, the 6-month period of November–April for SIO and SPA during the years of 1998/99–2005/06. TRMM 2A25 and 3B42 data are collected for these 8 half-year periods (8 TC seasons) for each basin.

Since in some basins, for example, NWP and SIO, TCs occur all year round, our selection of the 6-month period excludes some TC activity from the precipitation analysis. To evaluate how much TC activity is being excluded and where it is being excluded, in Fig. 3 we compare the yearly averaged accumulated cyclone energy (ACE; Bell et al. 2000) of the 8 seasons with those of the 8 entire years and a long-term record (30 entire years during 1979–2008). ACE is an index of TC activity. It is defined as the sum of the squares of the estimated 6-hourly maximum sustained surface wind speed for all TCs having tropical storm intensity or greater summed over all 6-h periods. As stated in Camargo and Sobel (2005), ACE is a very useful TC activity index because it is a continuous variable. Its integration of storm intensity over the lifetime of each storm as well as over all storms is appropriate for indexing the effect of TCs on climate, and therefore might be strongly correlated with TC precipitation. From Figs. 3a,b it can be seen that majority of TC activity during the 8 entire years is captured by the 8-season selection. However, it is also obvious that the 8-season selection missed some TC activity in each basin, especially in NWP as seen from Fig. 3d, which shows the difference between Figs. 3a,b. In NWP basin, up to 20% ACE is missed in a small region east of the Philippine Islands. There are also some

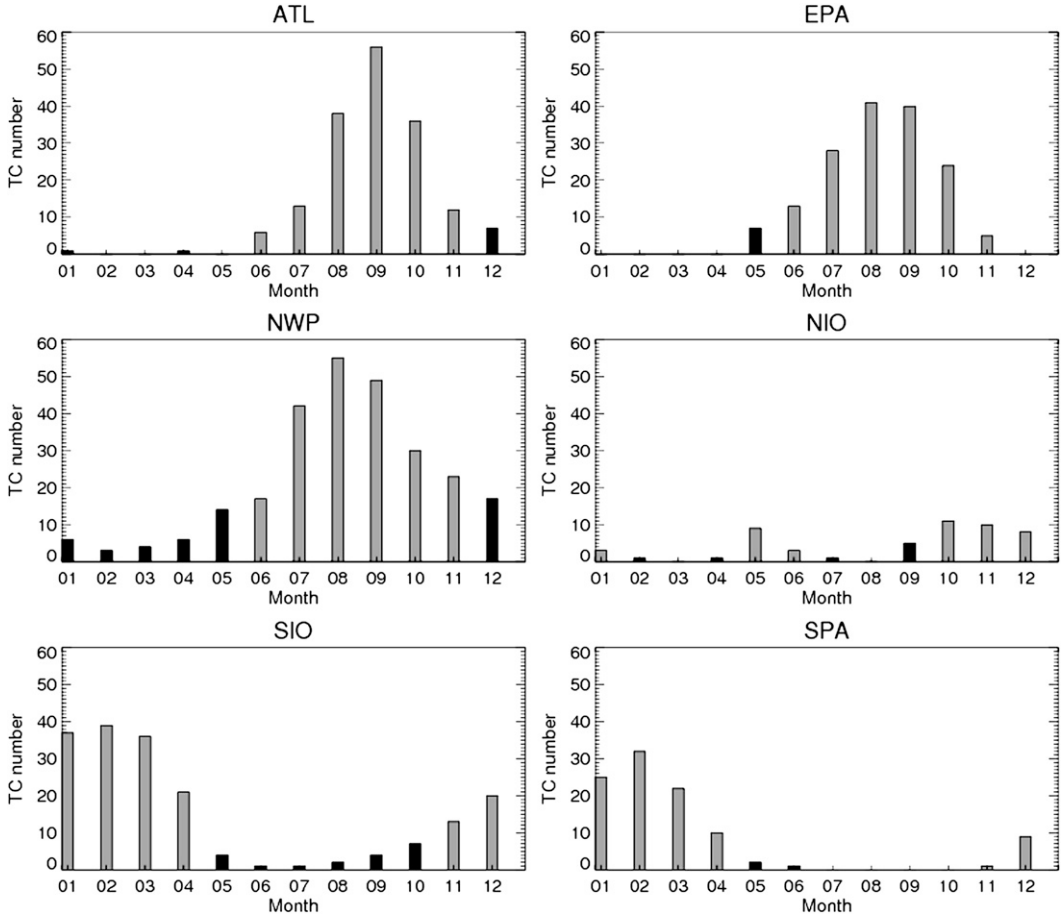

FIG. 2. Monthly TC numbers in each basin during 1998–2006 as derived from NHC and JTWC best-track data. Months that are used in the analysis are in gray, and all other months are in black.

other minimal missing areas in each basins. Compared with the 30 years of long-term record (Figs. 3c,e), the 8-season ACE shows a very similar pattern with slightly different magnitude. The 30-year ACE is greater than the 8-season ACE by up to 20%–25% in some areas in NWP and EPA, but there are also some areas (east of Taiwan Island, the Australia west coast, and almost the whole ATL basin) where 8-season ACE is greater.

During the analysis period, 606 (607) TCs that reached storm stage (maximum wind speed > 17 m s^{-1}) and greater were observed globally, providing 7582 (34 500) instantaneous observations by TRMM PR 2A25 (3B42). Observations over tropical depression stages are also included for storms whose maximum intensities are up to tropical storm or greater. To determine if the TRMM 2A25 dataset is representative of the distribution of TCs in terms of the sample size over the analysis period, the number of observations by 2A25 was compared to that by the 3-hourly 3B42 product. Table 1 shows a summary of the TC, observation, and PF numbers and percentage of 2A25 and 3B42 observations in each intensity and basin group for the analysis period of 8 half years. The 3B42 and 2A25 distributions are similar in general in Table 1, although the absolute numbers of observations from 3B42 are much larger (about a factor of $4 \sim 5$) than 2A25. The 2A25 dataset is slightly biased toward stronger storms in the northwest Pacific, as 39% (28.5%) of 2A25 observations are from typhoons (tropical depressions) compared to 35.5% (32.5%) of the 3B42 observations. All other basins show a difference of percentages in all intensity categories equal or less than 2% between 2A25 and 3B42. The percentage of total 2A25 numbers of observations is higher than 3B42 in ATL, NWP, and SPA, and lower in EPA, NIO, and SIO, and equal to it in NIO and SPA. But the difference is equal to or less than 4%. In terms of number of storms, 2A25 missed only one TC (in EPA) during the 8-half-year analysis period compared to 3B42. In summary, similar to the 3B42 dataset, 2A25 is representative of the global TC activity in terms of sampling size.

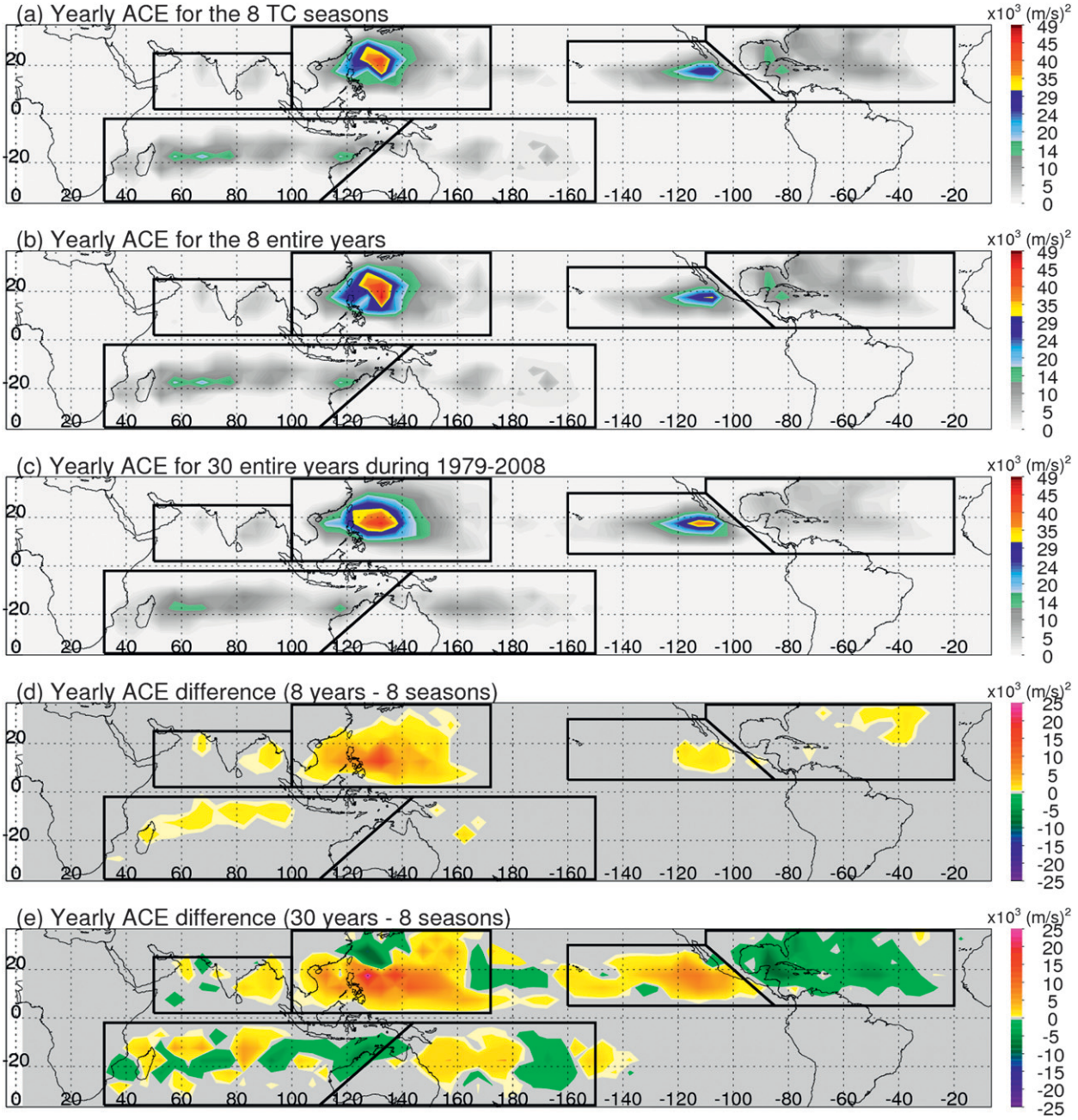

FIG. 3. Yearly ACE for (a) the 8 TC seasons in each basin (see text for details), (b) the 8 entire years, and (c) 30 entire years during 1979–2008; yearly ACE differences between (d) the 8 entire years and 8 TC seasons and (e) the 30 entire yeas and 8 TC seasons. Borders of six basins (ATL, EPA, NWP, NIO, SIO, and SPA) are indicated.

c. *Analysis methods*

TCPFs are determined based on a criterion that the distance between the center of TC and the center of the PF is within 500 km. From Table 1, we can see that on average 2A25 has about 20 TCPFs per TC observation, while 3B42 has only 5 (2A25 has 145 806 PFs in 7582 observations, while 3B42 has 169 186 PFs in 34 500 observations). The 3B42 features are usually much larger than 2A25 features because the spatial resolution of 2A25 (4.3 × 4.3 km before TRMM boost and 5.0 × 5.0 km after TRMM boost) is about 4–5 times higher than that of 3B42 (0.25° × 0.25°). The outcome is that, in majority of the cases, the 2A25 TCPFs are wholly contained within the circular area of 500 km of a TC. However, in a certain amount of cases, 3B42 TCPFs go

TABLE 1. Comparison of TRMM 2A25 and 3B42 sampled numbers of TCs, observations, and PFs in each basin during the analysis period of this study (see text for details). Observations are also separated for each TC intensity group (Hur represents hurricane strength TC, TS represents tropical storm, and TD represents tropical depression). Percentages of total observations for each intensity group and each basin are shown in parentheses.

			Observations									
	TCs		Hur		TS		TD		Total		PFs	
Basin	2A25	3B42	2A25	3B42	2A25	3B42	2A25	3B42	2A25	3B42	2A25	3B42
ATL	118	118	575 (31)	2187 (30)	808 (43)	3212 (44)	494 (26)	1926 (26)	1877 (25)	7325 (21)	34 896	40 325
EPA	111	112	232 (23.5)	1436 (25)	382 (38.5)	2139 (37)	372 (38)	2186 (38)	986 (13)	5761 (16.5)	16 771	26 634
NWP	155	155	857 (39)	3314 (35.5)	720 (32.5)	2947 (32)	633 (28.5)	2988 (32.5)	2210 (29)	9249 (27)	45 039	45 146
NIO	37	37	32 (10)	150 (9)	128 (40)	664 (41)	161 (50)	819 (50)	321 (4)	1633 (5)	6321	7707
SIO	120	120	389 (25.5)	1970 (26)	533 (35)	2558 (34)	601 (39.5)	3052 (40)	1523 (20)	7580 (22)	30 744	36 302
SPA	65	65	175 (26.5)	803 (27)	238 (35.5)	1013 (34.5)	252 (38)	1136 (38.5)	665 (9)	2952 (8.5)	12 035	13 072
Total	606	607	2260 (30)	9860 (28.5)	2809 (37)	12 533 (36.5)	2513 (33)	12 107 (35)	7582	34 500	145 806	169 186

far beyond the 500-km circle. Figure 4 shows a typical example observed in Hurricane Bonnie (1998). The large raining region beyond 500-km circle in the 3B42 was from a precipitation system not associated the hurricane. This feature is separated with the hurricane feature in both 2A12 rain and 85-GHz PCT panels in Fig. 4. However, the 3B42 rain field shows only one continuous PF. Although there is only a slight overestimate of rain rate (from no rain to very light rain) by 3B42 in the connection area between the two features, it makes the 3B42 TCPF definition invalid in doing TC analysis here. The slight overestimation of 3B42 in no-rain regions is possibly caused by the combination of its low spatial resolution induced by microwave data and overestimation of rain in cold cloud regions induced by IR observations. Because of this circumstance, besides the 2A25 TCPF and 3B42 TCPF datasets, we built a 3B42 500-km dataset in which only the 3B42 rain rates that are observed within 500 km of the center of TCs are used for TC rains. The 3B42 500-km dataset has a much better coverage of a TC than 2A25. It could exclude some raining areas that are associated with the TC but go beyond 500-km radius, but this omission should only be a problem for a minimal number of TC observations (Larson et al. 2005). As expected, it is found that the 3B42 TCPF–derived TC rainfall has similar pattern but 1.5–3 times as much as its 2A25 TCPF and 3B42 500-km counterparts (not shown here). Therefore, in this paper, we will only compare 2A25 TCPF–derived results with 3B42 500 km.

To estimate the monthly TC rainfall for the 6 selected months each year, the rain rates derived from the 2A25 TCPF and 3B42 500-km datasets are accumulated and averaged for a 5° latitude–longitude grid and then multiplied by the number of hours for that given month. These values will be referred to as ''TC rainfall'' in the following text. Total rainfall and non-TC rainfall are calculated using the same procedure from all systems and non-TC systems, respectively, for the 6 selected months each year.

3. Geographical distribution

Figures 5a–d show, respectively, the geographical distribution of the 2A25 TCPF–derived mean monthly total rainfall, non-TC rainfall, TC rainfall, and the percentage of rainfall contributed by TCs during the TC season (see section 2b for the analysis period) for each basin. The general rainfall pattern and locations of greatest total rainfall and non-TC rainfall are similar as seen from Figs. 5a,b. Precipitation near the equator is high in part because of the influence of the intertropical convergence zone (ITCZ). At about 30° north and south latitude precipitation decreases because of the presence of the subtropical high pressure systems. The regions of greatest total and non-TC rainfall (>250 mm month^{-1}) are associated with the ITCZ, northwest Pacific monsoon trough, South Pacific convergence zone (SPCZ), India monsoon, and South American summer monsoon. Figure 5c suggests that the maximum TC mean monthly rainfall is concentrated at various locations in each basin. These TC rain maximum locations are very different from and poleward of, those for total–non-TC rains.

Figure 5d shows the TC rain percentage. It indicates that the maximum percentage is located either at the same place where the TC rain itself is concentrated (ATL, NWP, SIO, and NIO) or even more poleward than TC rain itself (EPA, NIO, and SIO). The peak of TC rain percentage is at 20°N in EPA basin, 19°–21°N in NIO, and 18°–19°S in SIO basin. Several coastal regions with greatest contribution of TC rainfall can be identified from Fig. 5d. The first one is in a region west of the Baja California coast (between 15° and 25°N and between 110° and 130°W) in EPA, where the maximum percentage of TC rain is above 55%. The second one is

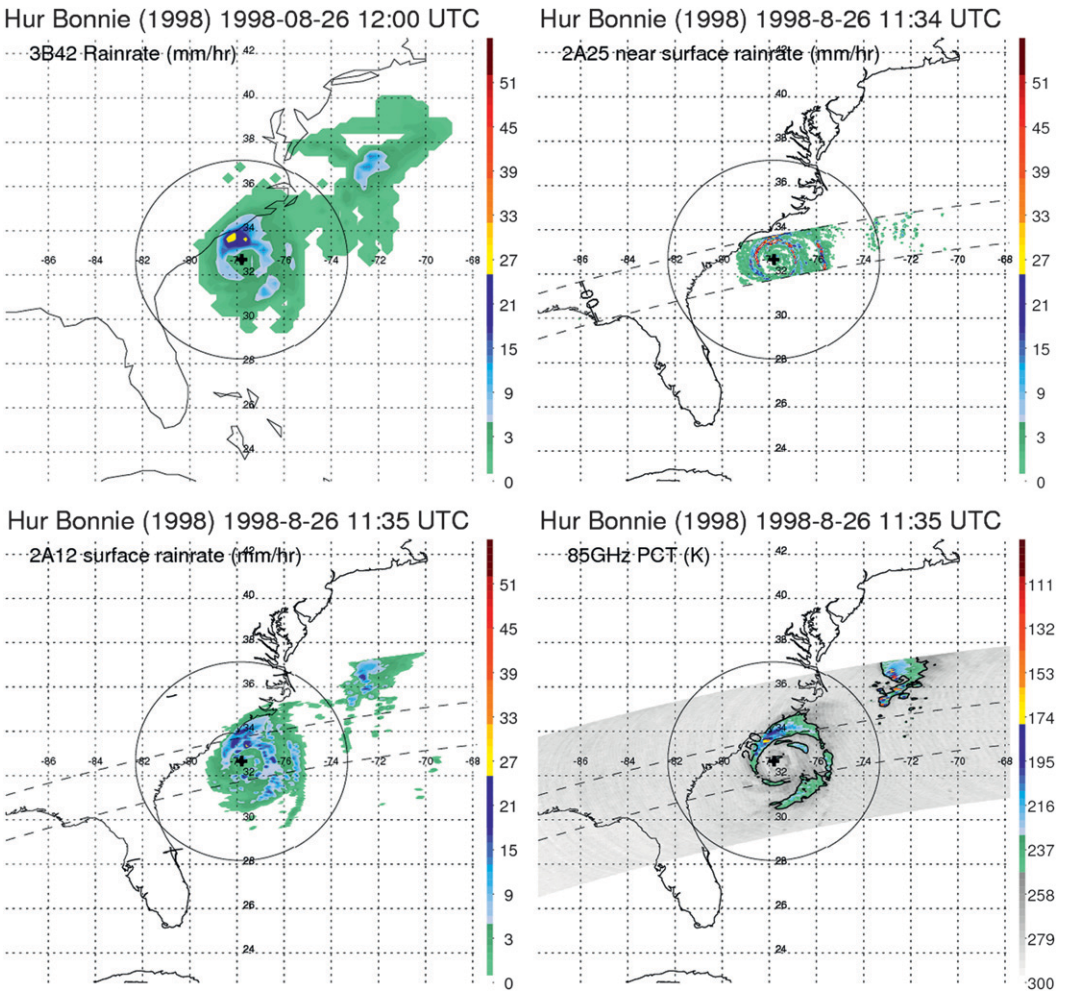

FIG. 4. The (top left) 3B42 rain rate at 1200 UTC, and (top right) 2A25 and (bottom left) 2A12 rain rates and (bottom right) 85-GHz PCT at near 1135 UTC on 26 Aug 1998 for Hurricane Bonnie. A 500-km radius circle around the storm center is indicated.

located west of the Australia coast (16°S and between 110° and 120°E) in SPA. The maximum percentage is also around 55%. The third percentage peak is in NWP within the region around Taiwan Island and northeast of the Philippine Islands where the rainfall contributed by TCs is approximately 35%–40%. It is believed that this area is associated with the North Pacific tropical upper-tropospheric trough (TUTT) where TCs usually intensify rapidly (Holiday and Thompson 1979). Rodgers et al. (2000) found a lower maximum percentage of TC rainfall over the Baja California (30%) and Taiwan Island region (10%–20%) by using 1987–98 Special Sensor Microwave Imager (SSM/I) data. The difference could perhaps be due to the retrieval algorithm difference between SSM/I and TRMM 2A25. The SSM/I-based rainfall retrieval may have missed or underestimated shallow orographic rainfall in coastal regions because the passive microwave technique is dependent on scattering from ice to produce the necessary liquid. Also the SSM/I algorithm used in Rodgers et al. (2001) was an old version of the microwave retrieval algorithm, while, in the version that 3B42 uses, several improvements have been made. On the other hand, our result for the TC rainfall percentage over Taiwan Island is closer to long-term rain gauge–based analyses by Ren et al. (2006) and Kubota and Wang (2009). Ren et al. (2006) found that the percentage of TC rainfall to annual total rain is between 30% and 45% in Taiwan, while Kubota and Wang (2009) found the ratio of TC rain to total rain during July–October is 50%–60% in Taiwan during 1951–2005.

Figure 5d also suggests that TCs contribute significantly to the rainfall over coastal areas in the Arabian Sea, Southeast Asia, southeast United States and Mexico, Caribbean Islands, Madagascar Island, and north coast

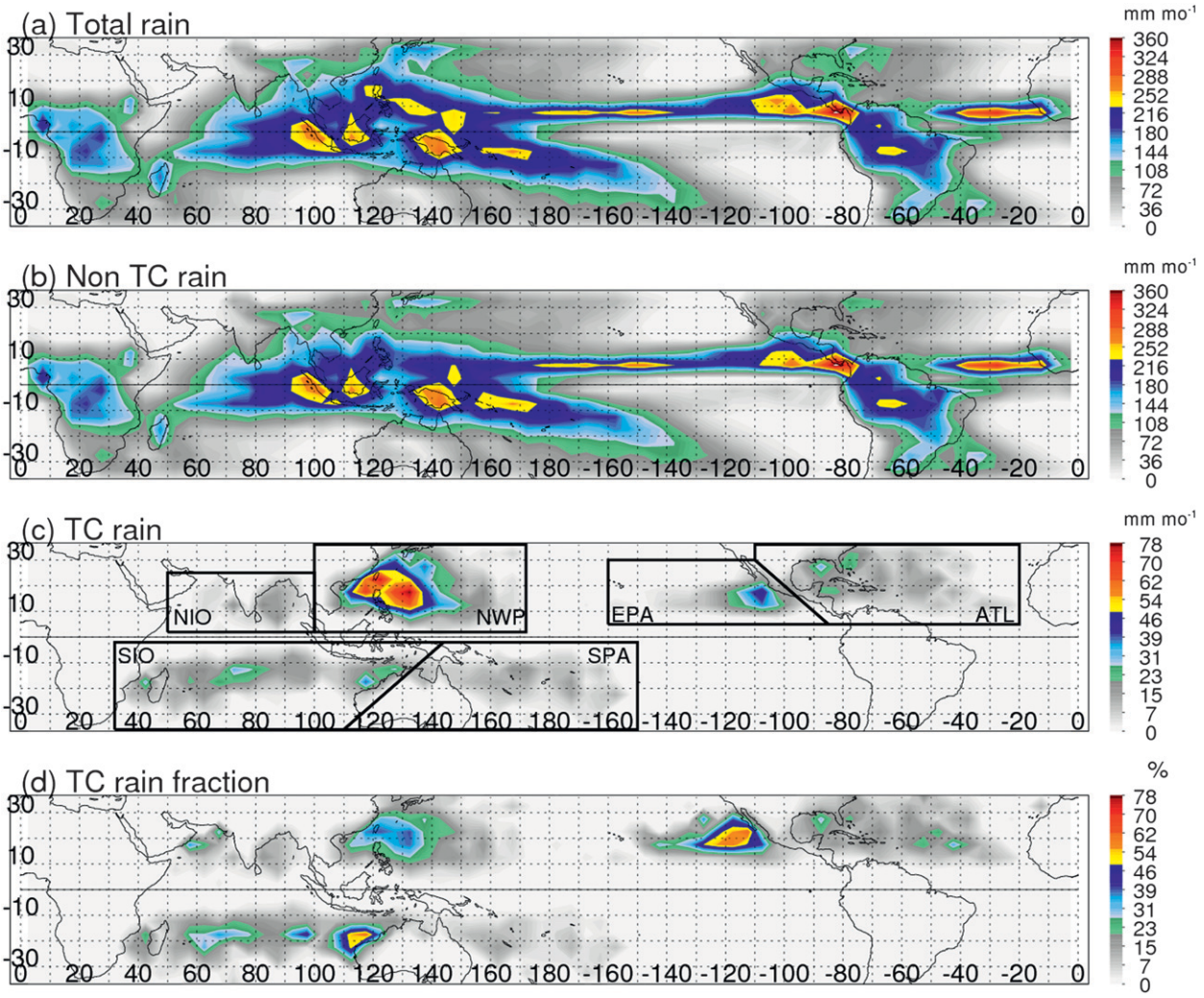

FIG. 5. The 2A25 (a) total rain, (b) non-TC rain, (c) TC rain, and (d) TC rain fraction based on 5° grid averages for the TC season (June–November for ATL, EPA, and NWP basins; May–June and October–January for the NIO basin) for the years of 1998–2000 and 2002–06 in the Northern Hemisphere and November–April for the years of 1998/99–2005/06 in the Southern Hemisphere. Borders of six basins (ATL, EPA, NWP, NIO, SIO, and SPA) are indicated in (c).

of Australia. In the Arabian Sea, TC contributes about 30% of total rain during NIO TC season over southeast coastal regions of Oman and south coastal regions of the Pakistan and Indian border. A 25% contribution due to TCs is evident in the northern islands of the Philippines and a small coastal region of southeast China, with a lower contribution (1%–20%) in the rest of Philippine Islands and the rest of southeast China including Hainan Island, central Vietnam, and southern Japan, and a much lower contribution (1%–5%) in eastern India. The Yucatan and Florida Peninsulas and Caribbean Islands also have significant TC rainfall (7%–20%), with the rest of southeast U.S. coastal regions and central Mexico having smaller percentages. As mentioned before, using rain gauge observations, Larson et al. (2005) found that up to 15% (20%) of summer precipitation along the U.S. Gulf Coast (Mexican coast) during 1950–98. This is very similar to what we found here (Fig. 5d). In the Southern Hemisphere, up to 40% of TC rainfall contribution is seen in western coast of Australia, with lower but significant values in northern coast of Australia (1%–10%) and Madagascar Island (5%–25%).

Comparing 3B42 and 2A25

For comparison, the geographical distributions of the 3B42 500-km–derived mean monthly total rainfall, non-TC rainfall, TC rainfall, and the percentage of rainfall contributed by TCs are presented in Fig. 6. The patterns of 3B42 500-km–derived parameters are similar to their 2A25 TCPF counterparts. The magnitudes of 3B42

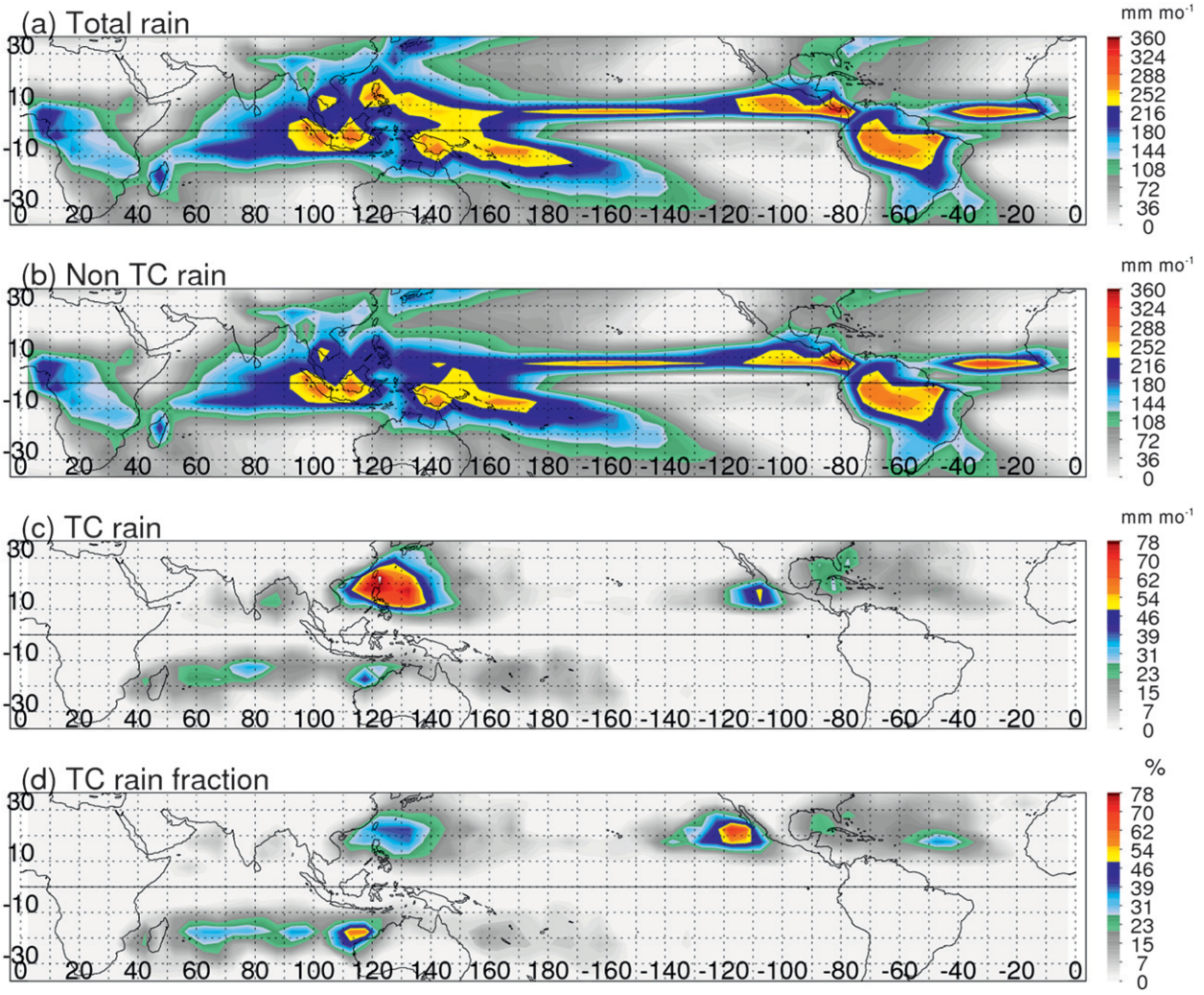

FIG. 6. As in Fig. 5, but rainfall amounts are derived from 3B42 500-km dataset (see text for details).

and 2A25 total rainfall and non-TC rainfall are similar over most regions, except that 3B42 is higher than 2A25 in South America and lower than 2A25 in southern Africa (Figs. 6a,b). The 3B42 500-km–derived TC rain and TC rain percentage (Figs. 6c,d) have magnitudes closer to 2A25 TCPF (Figs. 5c,d). The maximum 3B42 500-km–derived TC mean monthly rain is about 80 mm month^{-1} in Taiwan and the Philippines region.

A point-by-point comparison of 3B42 and 2A25 total rain and 3B42 500-km and 2A25 TCPF TC rain is shown in Fig. 7. It is obvious that the 3B42 and 2A25 total rains are close to each other. Similarly, the mean value of 3B42 500-km TC rain is 5.3 mm month^{-1}, which is very close to 2A25. A similar analysis using TMI-based 2A12 rain retrievals in PR swath has been done (not shown here), and it is found that 2A12 total rain and TC rain are all close to its 2A25 and 3B42 500-km counterparts in the time and space scale used in this study. Cecil and Wingo (2009) provided a more detailed comparison of 2A25 and 2A12 TC rain in a finer scale. They found that 2A25 produced more rain within ~100 km of the center of hurricanes compared to 2A12. However, at larger distances and for weaker storms, those two algorithms gave similar mean rain rates (slightly greater for 2A12). From their Fig. 2, the averages over 0–500 km and combining all storm intensities should be similar for 2A25 and 2A12.

Table 2 shows the basin-averaged total rain, non-TC rain, TC rain, and TC rain percentage derived from 2A25 TCPF and 3B42 500 km. Regardless which dataset is used, it can be seen from Table 2 that, among the six global TC basins, NWP has the highest non-TC and TC rain and TC rain fraction. SPA has the second highest non-TC rain, but lowest TC rain and TC rain fraction. NIO has the second lowest TC rain and TC rain fraction. ATL, EPA, and SIO have similar amounts of mean

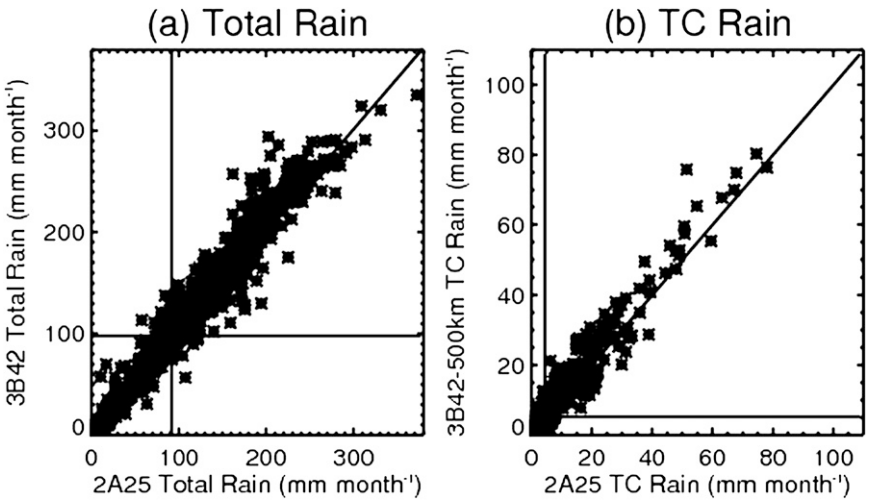

FIG. 7. The scatterplots for (a) 3B42 vs 2A25 total rain and (b) 3B42 500-km vs 2A25 TC rain. The monthly mean values are for the same time period as in Fig. 5 and represents 5° grids within 36°S and 36°N. The 1:1 line is indicated. The vertical and horizontal lines indicate the averages between 36°S and 36°N.

monthly TC rainfall/TC rainfall fraction and rank after NWP and before SPA and NIO. Also from Table 2, 3B42 500-km–derived TC rain and percentage TC rain are slightly higher than or equal to their 2A25 TCPF counterparts. In sections 4–6, we will only present 2A25 TCPF–derived results because they have similar patterns–magnitudes as their 3B42 counterparts.

From Figs. 5 and 6 and Table 2 we can see that NWP has greatest TC rainfall contribution among the six global TC basins. This is consistent with previous findings that NWP is the most active TC basin in both TC number and intensity. A large area of high SST and low wind shear in NWP are favorable to TC development (Gray 1968). Figure 8 shows the TC number density (how many storms passed any $1° \times 1°$ grid box) during 1998–2006 derived from NHC and JTWC best-track data. There are three peak regions with TC number greater than 18 in a $1° \times 1°$ grid box. One is in EPA near the west coast of Mexico. But its area is smaller than the total area of the other two peaks that are both in NWP. From Fig. 3 we can also see that the TC activity indicated by ACE is the greatest in NWP. Figure 9 presents the cumulative density functions (CDFs) of TC raining area and volumetric rain derived from the 3B42 500-km dataset during 1998–2006 for each basin. From Fig. 9, we find that NWP and SPA have the largest TC sizes as indicated by raining area with median values of 330 833 km^2 and 340 367 km^2, respectively, and by volumetric rain with median values of 895 304 km^2 mm h^{-1} and 842 541 km^2 mm h^{-1}, respectively. TCs in NIO and SIO are smaller and have less total volumetric rain, with median raining area of 251 459 km^2 and 281 318 km^2, respectively, and median volumetric rain of 656 208 km^2 mm h^{-1} and 623 230 km^2 mm h^{-1}, respectively. Storm sizes in ATL and EPA are usually the smallest with smallest volumetric rain. The median raining areas in ATL and EPA are 212 923 km^2 and 196 679 km^2, respectively. The median volumetric rains are 515 758 km^2 mm h^{-1} and 341 377 km^2 mm h^{-1}, respectively. Since NWP has the highest TC number density and largest TC size and volumetric rain, it explains why NWP TCs produce more precipitation than their counterparts in the other basins.

TABLE 2. The 2A25, 3B42 TCPF, and 3B42 500-km basin-averaged total rain, non-TC rain, TC rain, and TC rain fraction for the same time period as in Fig. 4.

	Total rain (mm $month^{-1}$)		Non-TC rain (mm $month^{-1}$)		TC rain (mm $month^{-1}$)		TC rain fraction (%)	
Basin	2A25	3B42	2A25 TCPF	3B42 500 km	2A25 TCPF	3B42 500 km	2A25 TCPF	3B42 500 km
ATL	100	102	93	93	8	9	8	9
EPA	105	111	98	103	7	8	7	7
NWP	155	170	137	151	17	19	11	11
NIO	102	105	97	100	5	5	5	5
SIO	101	109	95	101	7	8	7	8
SPA	118	128	114	123	4	5	3	4

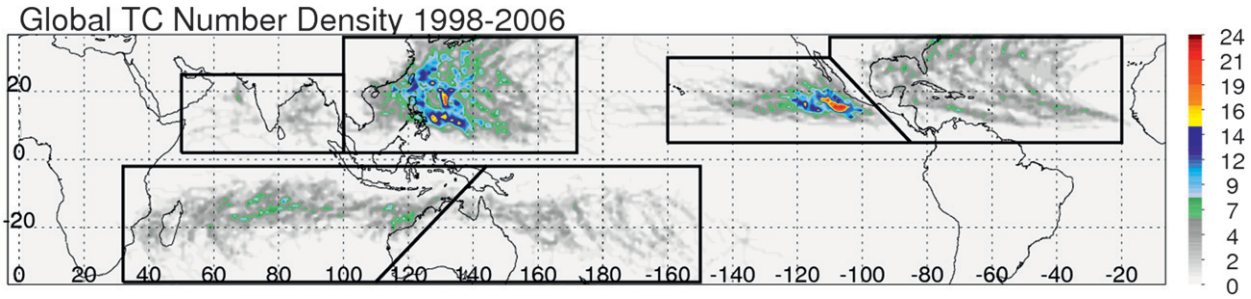

FIG. 8. Global TC number density on 1° × 1° grids during 1998–2006.

4. Rainfall and tropical cyclone intensity

The geographic distribution of TC rainfall contributed by hurricane strength TCs, tropical storms, and tropical depressions is seen in Fig. 10. Rainfall from typhoons extends to a large area in NWP and the peak is as high as 50 mm month^{-1} in a region east of the Philippines in the NWP basin. Rainfall from TCs of hurricane intensity is generally less than 20 mm month^{-1} in other basins. Rainfall from TCs in hurricane intensity is concentrated more poleward than storms and depressions for all basins. For example, peak hurricane rainfall is located at around 28°N in the ATL basin. Peak TC rainfall from hurricane-stage storms in SPA and SIO is located at 19°S. Storms with a longer life time often are able to travel to subtropical regions from lower latitudes and under favorable conditions may intensify in higher-latitude regions. Rainfall from tropical storms and depressions is generally less than 25 mm month^{-1} in NWP; 15 mm month^{-1} in EPA, NIO and SIO; and 12 mm month^{-1} in ATL and SPA.

The basin-averaged TC rainfall and percentage contributed by different intensity stages is presented in Table 3. The table shows that the greatest rain amounts observed during the analysis period in ATL, EPA, NWP, and SPA are contributed by TCs in hurricane stage, while the greatest rain amounts during this period are contributed by TCs in depression stage for the NIO basin and storm stage for the SIO basin. Depressions are relatively more frequent in the NIO than in other regions. For SIO, the implication is that either the tropical storm stage is more frequent, or that tropical storms (TSs) produce a larger total volumetric rain during the period along the western Australia coast than either depressions or strong tropical cyclones.

5. Seasonal variation of tropical cyclone rainfall

The seasonal variation of the Northern Hemisphere TC mean monthly rain for the months of May–January is presented in Fig. 11. We select this 9-month period to cover TC seasons in all basins in the Northern Hemisphere. The figure shows that ATL and EPA (NWP) TC rainfall increases from May to September (August) and then decreases after September (August). TC rain is zero in May and January for ATL and in December and January for EPA. NWP has TC activities all year long. NIO TC rainfall peaks in May and decreases from June to July,

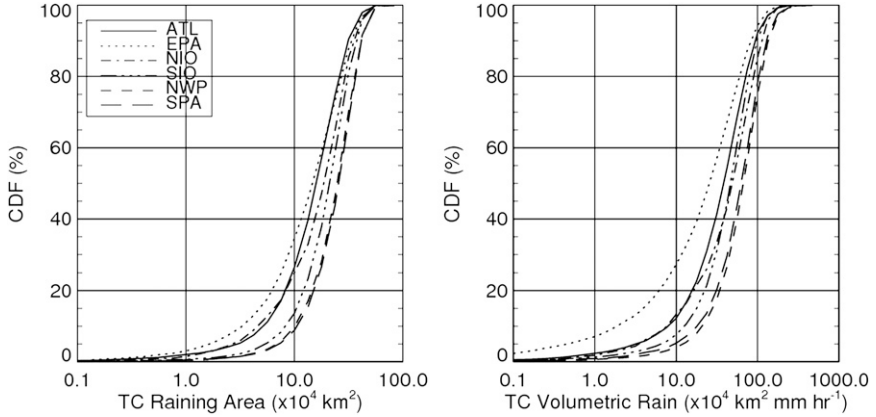

FIG. 9. CDFs of TC (left) raining area and (right) volumetric rain for each basin as derived from the 3B42 500-km dataset (see text for details).

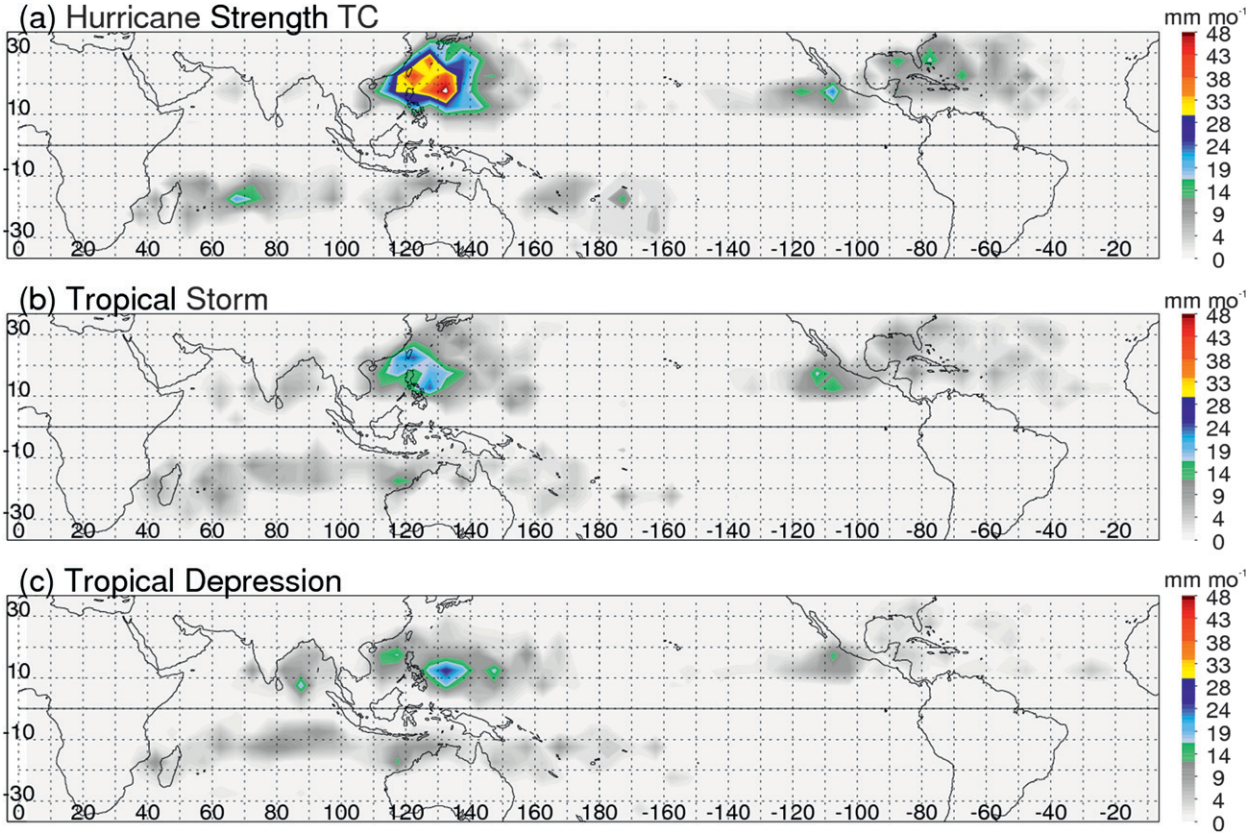

FIG. 10. The 2A25 (a) hurricane strength TC rain, (b) tropical storm rain, and (c) tropical depression rain based on 5° grid averages for the same time period as in Fig. 4.

is zero in August, and then increases from September to December, and decreases again from December to January. This is not surprising because it is well known that NIO TCs tend to have a break, as noted above, during the Indian monsoon period (July–September). The seasonal movement of rainfall centers is also very interesting. In NWP, TC rainfall is concentrated between 10° and 20°N in May–June, then moves northward to 15°–25°N in July, and becomes more widespread and extends to 15°–30°N in August. After August, the center of TC rainfall moves southward gradually and is back to 12°N in November–December. In ATL, TC rain is concentrated in the Gulf of Mexico region between 15° and 30°N and 80° and 90°W in June. In July, it extends to the eastern Mexico coast and the western Caribbean Sea. In August and September, as the TC rain amount increases, the TC rain region spreads to the entire basin including the eastern North Atlantic. The center is located between 20° and 30°N in September. Thereafter, as TC rain decreases, the rain center moves southward and is between 10° and 20°N in October and November. This zonal shift of TC rainfall in both NWP and ATL is mainly due to the variation of climatological low wind shear/high SST region from early summer to late summer (Gray 1968; Chen et al. 2006).

In EPA, TC rainfall focuses between 10° and 20°N through most of the season, which is due to the lack of zonal shift of SSTs in this region (Rodgers et al. 2000). TC rainfall in EPA is mainly confined to the east of 120°W, with small extension westward from July to October. As Gray (1968) pointed out, the increasingly larger vertical wind shear west of 120°W produces a less favorable environment for TC development.

TABLE 3. The 2A25 basin-averaged TC rain and rain fraction contributed by TCs in Hur, TS, and TD stages for the same time period as in Fig. 4.

	Rain (mm month^{-1})			Rain fraction (%)		
Basin	Hur	TS	TD	Hur	TS	TD
ATL	3.6	2.9	1.4	3.6	2.9	1.4
EPA	2.6	2.5	1.9	2.4	2.4	1.8
NWP	8.2	5.1	4.2	5.3	3.3	2.7
NIO	0.6	1.8	2.2	0.6	1.8	2.2
SIO	2.2	2.3	2.2	2.2	2.3	2.2
SPA	1.6	1.3	1.2	1.3	1.1	1.1

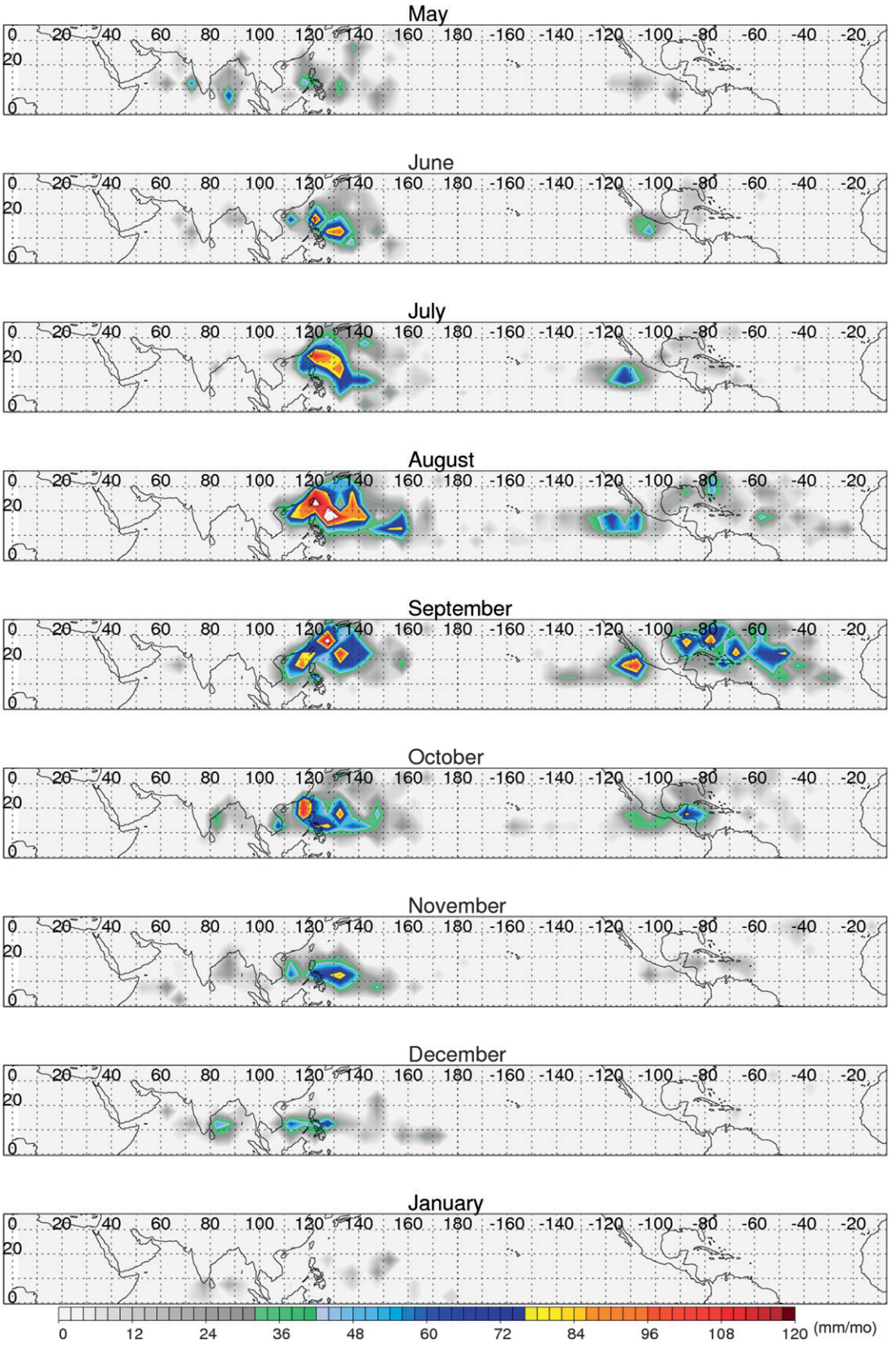

FIG. 11. Seasonal 2A25 TC rain fraction based on 5° grid averages for the months of May–January for the years of 1998–2000 and 2002–06 in the Northern Hemisphere.

In NIO, TC rain occurs from 20°N to 0° in May in the Bay of Bengal and 10° to 20°N in the Arabian Sea, and then decreases in both area and magnitude in June. Only a small area on the eastern India coast is found in July and even that disappears in August. Then TC rainfall reappears in the middle of Arabian Sea in September and moves to the eastern India, eastern Myanmar, and southern Bangladesh coasts in October. From November to January, TC rainfall moves southward decreases in areal coverage.

The seasonal variation of the Southern Hemisphere TC mean monthly rain for the months of November–April is presented in Fig. 12. The figure shows that SIO (SPA) TC rainfall increases from November to March (January) and then decreases. No TC occurs in November in SPA during the analysis period. The maxima west of the Australia coast and west of Madagascar Island are present from December through April with only slight shifts in location. The maximum in the central south Indian Ocean occurs in all the months with large latitudinal and longitudinal variation. In SPA there is a major increase from December to January and a decrease from March to April.

Figure 13 shows a bar graph that indicates the seasonal variation of the non-TC (shaded bars) and TC (white bars) mean monthly rainfall amounts for months of May–January for Northern Hemisphere basins and November–April for Southern Hemisphere basins. The TC mean monthly rainfall and the percentage of rainfall contributed by TCs both peak in September in ATL, August–September in EPA, August in NWP, May in NIO, March in SIO, and January–February in SPA. In the Pacific (including EPA, NWP, and SPA), the months that contain the greatest TC rainfall amounts–percentages coincide with the months that have the largest non-TC rainfall. Rodgers et al. (2000) found the same coincidence in EPA. However, in ATL the month with greatest TC rainfall (i.e., September) precedes with the month with greatest non-TC rainfall (i.e., October). Rodgers et al. (2001) found the same off phase between TC and non-TC rainfall in eastern ATL, while in western ATL the months with the greatest TC and non-TC rainfall coincide with each other. This suggests that the ATL TC rainfall is dominated by the eastern ATL storms generated by the African easterly waves (Landsea and Gray 1992). In NIO (SIO), the maximum TC rainfall occurs in May (March) and precedes (lags) the maximum non-TC rainfall which occurs in June (January).

6. Interannual variation of tropical cyclone rainfall

ENSO is the strongest interannual climate phenomenon on a global scale. ENSO is known to affect the year-to-year variability in TCs around the globe (Landsea 2000). Some previous studies have shown that there are fewer Atlantic hurricanes in an El Niño year than usual, while in a La Niña year there more Atlantic hurricanes (Gray 1984; Saunders et al. 2000). During an El Niño year, the wind shear is larger in most of the tropical Atlantic, which inhibits the formation of hurricanes. Rodgers et al. (2001) found an increase in ATL TC rainfall in La Niña years. The situation is a little complicated in the NWP. Mohr et al. (2009) showed that the probability of the occurrence of large organized convective systems does not change with the phase of ENSO. Lander (1994) did not observe an ENSO effect on annual typhoon numbers. However, many other studies (Chan 1985, 2000; Chan et al. 1998; Saunders et al. 2000) showed that the TC activity is above normal in the eastern part of the NWP and slightly below normal over the South China Sea during an El Niño event. They also found that TC activity during a La Niña event is almost exactly the reverse of those in El Niño years, with significantly below (above) normal activity over the eastern part of the NWP (South China Sea). Rodgers et al. (2000) suggested an increase in TC rainfall, frequency, and intensity in all of the North Pacific Ocean (including the NWP and EPA basins) during the warm ENSO years. Conflicting results have been presented for the NIO too. Some studies showed that TC activity in the NIO basin is not affected (Raghavan and Rajesh 2003), while others argued that there is a reduction in TC activity in intense cyclone months of May and November during El Niño years (O. P. Singh 2009, personal communication). Kuleshov et al. (2008) examined the 1981/82 to 2005/06 TC seasons in the Southern Hemisphere and found a higher annual TC numbers in La Niña years than El Niño years for the entire hemisphere (29 versus 25).

In this study, the multivariate ENSO index (MEI; Wolter 1987) is used to identify El Niño and La Niña years (http://www.cdc.noaa.gov/people/klaus.wolter/MEI/table.html). Each basin is considered separately based on the analyzed TC months indicated in section 2.2. A warm (cold) ENSO episode was identified using a MEI threshold of + (−) 0.55. The threshold is selected based on probability MEI ranks similar to Kuleshov et al. (2008). As a result, for the Northern Hemisphere basins, 2002 and 2006 are considered as El Niño years, while 1999 is considered as La Niña year. For the Southern Hemisphere, El Niño years are 2003 and 2005, while La Niña years are 1999 and 2000. The resulting El Niño and La Niña years are identical to those of Kuleshov et al. (2008) for the Southern Hemisphere during the period applicable to this study.

Figure 14 presents the differences of non-TC and TC rain between the El Niño and La Niña years. Figure 14a

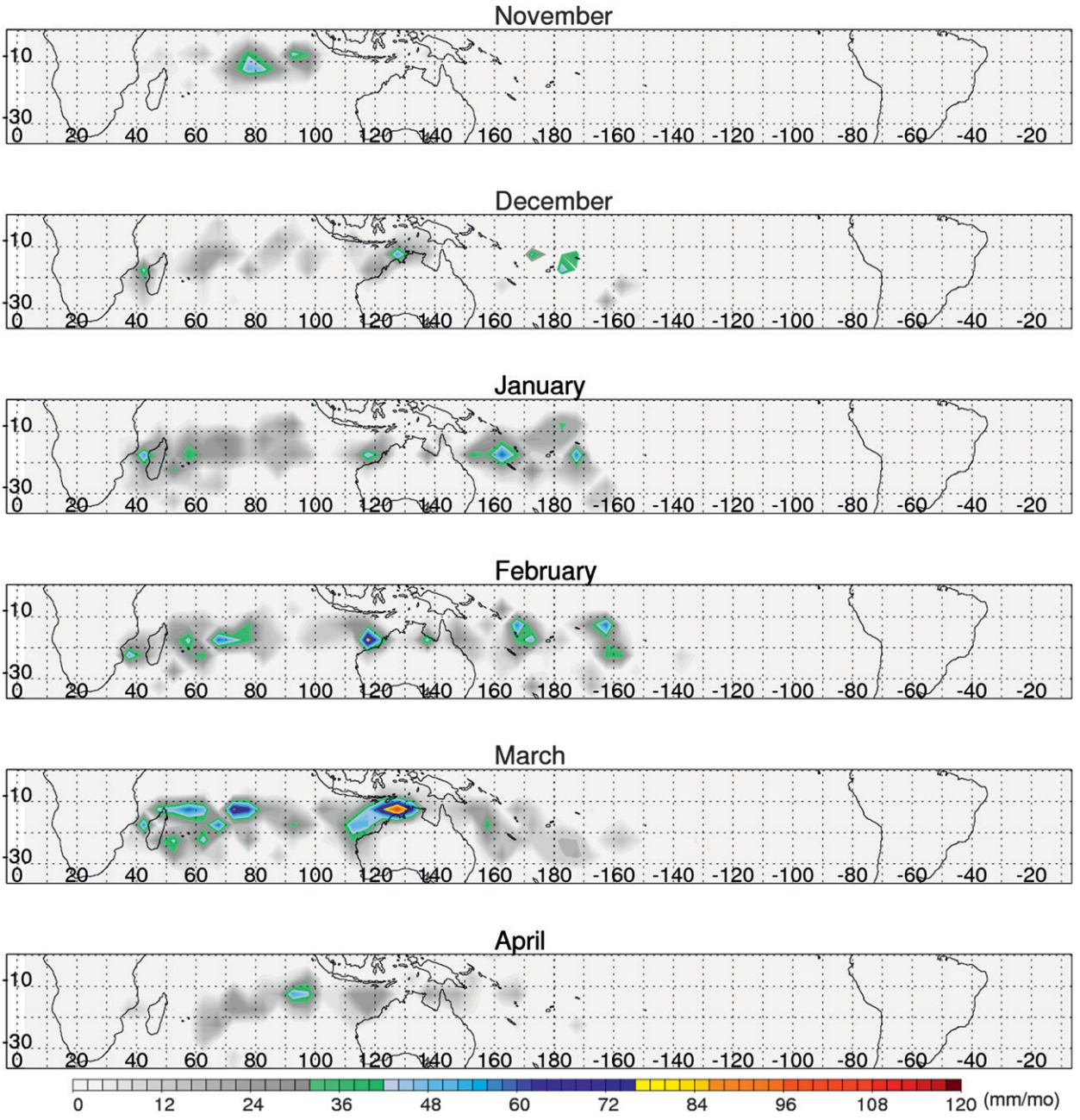

FIG. 12. Seasonal 2A25 TC rain fraction based on 5° grid averages for the months of November–April for the years of 1998/99–2005/06 in the Southern Hemisphere.

reveals that during the El Niño years there is a substantial increase in non-TC rainfall within the ITCZ across the North Atlantic, eastern North Pacific, and central Pacific and extending to 140°E and a smaller increase in the entire Indian Ocean (south and north). On the other hand, there is less non-TC rainfall during the El Niño years in a south–north band along 120°–140°E from the equator to over 20°N around the Philippines Islands in the Northern Hemisphere. The SPCZ (an east–west band along 10°–20°S from 90°E past the date line to 160°W) has an eastward shift during the El Niño years.

Figure 14b clearly shows that the TC rain is greater during the El Niño years in the EPA, most of the NWP, Gulf of Mexico, and western part (west of 90°W) of the SIO, southern part of NIO, and eastern part of SPA. On the other hand, TC rainfall is less during the El Niño years over the majority of the ATL, part of South China Sea around Taiwan and the Philippine Islands, Australia

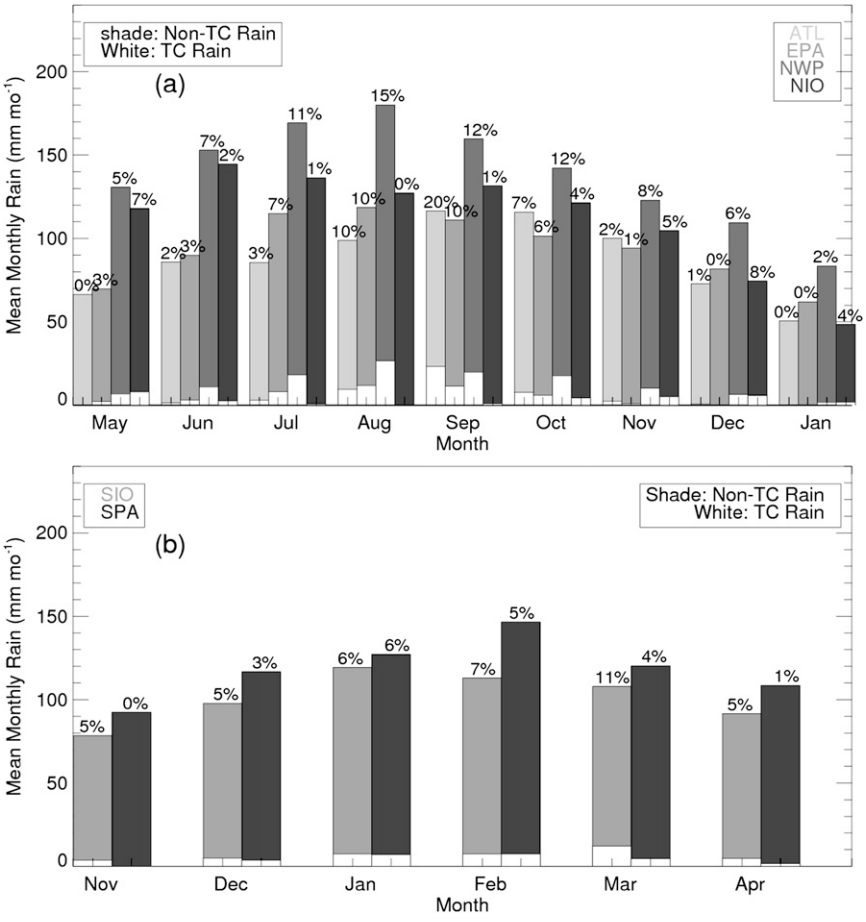

FIG. 13. A histogram showing the 2A25 basin-averaged mean monthly rainfall amounts contributed by non-TC systems (shade) and TCs (white) for (a) the months of May–January for the years of 1998–2000 and 2002–06 in the Northern Hemisphere basins and (b) the months of November–April for the years of 1998/99–2005/06 in the Southern Hemisphere. Percentage above the bar represents the percentage of rainfall contributed by TCs during the month.

west coast region, and south coast of India in Bay of Bengal. The result in Fig. 14 is generally consistent with Rodgers et al. (2000, 2001) but with some exceptions such as in the Gulf of Mexico and South China Sea. Neither this study nor Rodgers et al. (2000, 2001) include enough years of data to expect for the findings to be considered representative of long-term statistics.

7. Conclusions

The impacts of TCs on geographical, seasonal, and interannual variability of the total rainfall over six global basins are investigated using rainfall estimated from TRMM 2A25 and 3B42 during 1998–2006. The pattern of 3B42 TC rainfall is similar to its 2A25 counterpart, although the feature-based 3B42 TC rainfall (3B42 TCPF) overestimates about a factor of 2 relative to 2A25. By constraining TC rainfall within 500 km of a TC center, 3B42-derived TC rain and TC rainfall percentage are either slightly higher than or equal to its 2A25 counterparts.

TCs contribute, respectively, 11%, 8%–9%, 7%–8%, 7%, 5%, and 3%–4% of the total rainfall to the entire domain of NWP, ATL, SIO, EPA, NIO, and SPA basins during the TC season. The NWP basin has the highest TC rain and TC rain fraction because the TC number density and size in NWP are the highest and largest among the six basins. At smaller subbasin scales, the greatest contribution of TC rainfall is identified southwest of the Baja California coast (55%), west of the Australia coast (55%), and the region around Taiwan Island and northeast of the Philippine Islands (35%–40%).

Generally TC rain maximum locations are poleward of those for total/non-TC rains. The maximum TC rain percentage is at the same place as where the TC rain is concentrated in the ATL, NWP, and SIO basins, while it is poleward of the TC rain itself in the EPA, NIO, and SIO.

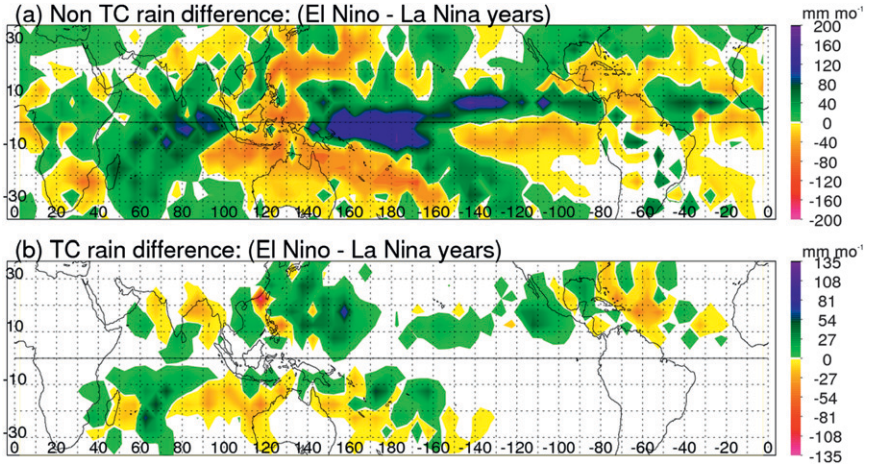

FIG. 14. The difference between (a) TC and (b) non-TC rain during El Niño years (2002 and 2004 for the Northern Hemisphere TC season and 2003 and 2005 for the Southern Hemisphere TC season) minus the La Niña years (1999 for the Northern Hemisphere TC season and 1999 and 2000 for the Southern Hemisphere TC season) derived from 2A25.

TCs of hurricane intensity contribute the greatest rain amounts in the ATL, EPA, NWP, and SPA basins, while tropical depressions (tropical storms) contribute the greatest rain amounts in the NIO (SIO) basin. Over the globe, the rainfall of hurricane-stage TCs is more poleward than that of depression and storm-stage TCs.

The seasonal TC rainfall shows different patterns for different basins. The percentage of TC rainfall peaks in September in the ATL basin (20%), August in NWP (15%), August and September in EPA (10%), February in SIO (7%), May in NIO (7%), and January in SPA (6%). The peak TC rainfall month usually overlaps with the month of peak TC rain fraction and sometime is offset with the peak month of TC numbers shown in Fig. 2.

Distinct differences in both TC and non-TC rainfall variations are shown between the El Niño and La Niña years. Substantial (slight) El Niño year increase of TC rain and TC rain fraction is seen for the NWP and EPA (SIO and SPA) basins, while a decrease in TC rainfall and TC rainfall percentage is found for the ATL and NIO basins. However, this study does not include enough years of data to expect the findings to be representative of long-term statistics.

Acknowledgments. We thank Dan Cecil and George Huffman for their very helpful review comments. Support for this study is provided by the NASA Precipitation Measurement Mission (PMM) Grant NNX07AL41G, NASA New Investigator Program (NIP) Grant NNX08AT20G, and NASA Hurricane Science Research Program (HSRP) Grant NNX09AC42G. The authors thank Ramesh Kakar and Ming-Ying Wei (NASA headquarters) for their support. Discussions with Bin Wang at University Hawaii, Bill Lau and Yaping Zhou at NASA Goddard, Chuntao Liu at University of Utah, and Fumin Ren at Chinese National Climate Center were very helpful.

REFERENCES

Adler, R. F., G. J. Huffman, D. T. Bolvin, S. Curtis, and E. J. Nelkin, 2000: Tropical rainfall distributions determined using TRMM combined with other satellite and rain gauge information. *J. Appl. Meteor.,* **39,** 2007–2023.

Bell, G. D., and Coauthors, 2000: Climate assessment for 1999. *Bull. Amer. Meteor. Soc.,* **81,** S1–S50.

Camargo, S. J., and A. H. Sobel, 2005: Western North Pacific tropical cyclone intensity and ENSO. *J. Climate,* **18,** 2996–3006.

Cecil, D. J., and E. J. Zipser, 2002: Reflectivity, ice scattering, and lightning characteristics of hurricane eyewalls and rainbands. Part II: Intercomparison of observations. *Mon. Wea. Rev.,* **130,** 785–801.

——, and M. Wingo, 2009: Comparison of TRMM rain rate retrievals in tropical cyclones. *J. Meteor. Soc. Japan,* **87A,** 369–380.

——, E. J. Zipser, and S. W. Nesbitt, 2002: Reflectivity, ice scattering, and lightning characteristics of hurricane eyewalls and rainbands. Part I: Quantitative description. *Mon. Wea. Rev.,* **130,** 769–784.

——, S. J. Goodman, D. J. Boccippio, E. J. Zipser, and S. W. Nesbitt, 2005: Three years of TRMM precipitation features. Part I: Radar, radiometric, and lightning characteristics. *Mon. Wea. Rev.,* **133,** 543–566.

Chan, J. C. L., 1985: Tropical cyclone activity in the northwest Pacific in relation to the El Niño/Southern Oscillation phenomenon. *Mon. Wea. Rev.,* **113,** 599–606.

——, 2000: Tropical cyclone activity over the western North Pacific associated with El Niño and La Niña Events. *J. Climate,* **13,** 2960–2972.

——, J. E. Shi, and C. M. Lam, 1998: Seasonal forecasting of tropical cyclone activity over the western North Pacific and the South China Sea. *Wea. Forecasting,* **13,** 997–1004.

Chen, S. S., J. A. Knaff, and F. D. Marks, 2006: Effects of vertical wind shear and storm motion on tropical cyclone rainfall asymmetries deduced from TRMM. *Mon. Wea. Rev.,* **134,** 3190–3208.

Gan, M. A., V. E. Kousky, and C. F. Ropelewski, 2004: The South America monsoon circulation and its relationship to rainfall over west-central Brazil. *J. Climate,* **17,** 47–66.

Gray, W. M., 1968: Global view of the origin of tropical disturbances and storms. *Mon. Wea. Rev.,* **96,** 669–700.

——, 1984: Atlantic seasonal hurricane frequency. Part I: El Niño and 30-mb Quasi-Biennial Oscillation influences. *Mon. Wea. Rev.,* **112,** 1649–1668.

Holiday, C. R., and A. H. Thompson, 1979: Climatological characteristics of rapidly intensifying typhoons. *Mon. Wea. Rev.,* **107,** 1022–1034.

Huffman, G. J., and Coauthors, 2007: The TRMM Multisatellite Precipitation Analysis (TMPA): Quasi-global, multiyear, combined-sensor precipitation estimates at fine scales. *J. Hydrometeor.,* **8,** 38–55.

Iguchi, T., T. Kozu, R. Meneghini, J. Awaka, and K. Okamoto, 2000: Rain-profiling algorithm for the TRMM precipitation radar. *J. Appl. Meteor.,* **39,** 2038–2052.

Kubota, H., and B. Wang, 2009: How much do tropical cyclones affect seasonal and interannual rainfall variability over the western North Pacific? *J. Climate,* **22,** 5495–5510.

Kuleshov, Y., L. Qi, R. Fawcett, and D. Jones, 2008: On tropical cyclone activity in the Southern Hemisphere: Trends and the ENSO connection. *Geophys. Res. Lett.,* **35,** L14S08, doi:10.1029/2007GL032983.

Kummerow, C., W. Barnes, T. Kozu, J. Shiue, and J. Simpson, 1998: The Tropical Rainfall Measuring Mission (TRMM) sensor package. *J. Atmos. Oceanic Technol.,* **15,** 809–817.

Lander, M. A., 1994: An exploratory analysis of the relationship between tropical storm formation in the western North Pacific and ENSO. *Mon. Wea. Rev.,* **122,** 636–651.

Landsea, C. W., 2000: El Niño/Southern Oscillation and the seasonal predictability of tropical cyclones. *El Niño and the Southern Oscillation: Multiscale Variability and Global and Regional Impacts,* H. F. Diaz and V. Markgraf, Eds., Cambridge University Press, 149–181.

——, and W. Gray, 1992: The strong association between western Sahelian monsoon rainfall and intense Atlantic hurricanes. *J. Climate,* **5,** 435–453.

Larson, J., Y. Zhou, and R. W. Higgins, 2005: Characteristics of landfalling tropical cyclones in the United States and Mexico: Climatology and interannual variability. *J. Climate,* **18,** 1247–1262.

Liu, C., E. J. Zipser, D. J. Cecil, S. W. Nesbitt, and S. Sherwood, 2008: A cloud and precipitation feature database from 9 years of TRMM observations. *J. Appl. Meteor. Climatol.,* **47,** 2712–2728.

Mohr, K. I., J. Molinari, and C. D. Thorncroft, 2009: The interannual stability of cumulative frequency distributions for convective system size and intensity. *J. Climate,* **22,** 5218–5231.

Mutai, C. C., and M. N. Ward, 2000: East African rainfall and the tropical circulation/convection on intraseasonal to interannual timescales. *J. Climate,* **13,** 3915–3939.

Nesbitt, S. W., E. J. Zipser, and D. J. Cecil, 2000: A census of precipitation features in the tropics using TRMM: Radar, ice scattering, and lightning observations. *J. Climate,* **13,** 4087–4106.

——, ——, and C. D. Kummerow, 2004: An examination of version-5 rainfall estimates from the TRMM microwave imager, precipitation radar, and rain gauges on global, regional, and storm scales. *J. Appl. Meteor.,* **43,** 1016–1036.

Raghavan, S., and S. Rajesh, 2003: Trends in tropical cyclone impact: A study in Andhra Pradesh, India. *Bull. Amer. Meteor. Soc.,* **84,** 635–644.

Ren, F., G. Wu, W. Dong, X. Wang, Y. Wang, W. Ai, and W. Li, 2006: Changes in tropical cyclone precipitation over China. *Geophys. Res. Lett.,* **33,** L20702, doi:10.1029/2006GL027951.

Rodgers, E. B., R. F. Adler, and H. F. Pierce, 2000: Contribution of tropical cyclones to the North Pacific climatological rainfall as observed from satellites. *J. Appl. Meteor.,* **39,** 1658–1678.

——, ——, and ——, 2001: Contribution of tropical cyclones to the North Atlantic climatological rainfall as observed from satellites. *J. Appl. Meteor.,* **40,** 1785–1800.

Saunders, M. A., R. E. Chandler, C. J. Merchant, and F. P. Roberts, 2000: Atlantic hurricanes and NW Pacific typhoons: ENSO spatial impacts on occurrence and landfall. *Geophys. Res. Lett.,* **27,** 1147–1150.

Schumacher, C., and R. A. Houze, 2003: Stratiform rain in the tropics as seen by the TRMM precipitation radar. *J. Climate,* **16,** 1739–1756.

Shepherd, J. M., A. Grundstein, and T. L. Mote, 2007: Quantifying the contribution of tropical cyclones to extreme rainfall along the coastal southeastern United States. *Geophys. Res. Lett.,* **34,** L23810, doi:10.1029/2007GL031694.

Simpson, J., R. F. Adler, and G. R. North, 1988: A proposed Tropical Rainfall Measuring Mission (TRMM) satellite. *Bull. Amer. Meteor. Soc.,* **69,** 278–295.

Spencer, R. W., H. M. Goodman, and R. E. Hood, 1989: Precipitation retrieval over land and ocean with the SSM/I: Identification and characteristics of the scattering signal. *J. Atmos. Oceanic Technol.,* **6,** 254–273.

Wolter, K., 1987: The southern oscillation in surface circulation and climate over the tropical Atlantic, eastern Pacific, and Indian Oceans as captured by cluster analysis. *J. Appl. Meteor.,* **26,** 540–558.

Wu, Y., S. Wu, and P. Zhai, 2007: The impact of tropical cyclones on Hainan Island's extreme and total precipitation. *Int. J. Climatol.,* **27,** 1059–1064.

Yokoyama, C., and Y. N. Takayabu, 2008: A statistical study on rain characteristics of tropical cyclones using TRMM satellite data. *Mon. Wea. Rev.,* **136,** 3848–3862.

Zipser, E. J., D. J. Cecil, C. Liu, S. W. Nesbitt, and D. P. Yorty, 2006: Where are the most intense thunderstorms on earth? *Bull. Amer. Meteor. Soc.,* **87,** 1057–1071.